

Accelerating Physics-Based Electromigration Analysis via Rational Krylov Subspaces

Sheldon X.-D. Tan, *Fellow, IEEE* and Haotian Lu, *Student Member, IEEE*

Department of Electrical and Computer Engineering, University of California at Riverside, Riverside, CA

Abstract—Electromigration (EM)-induced stress in interconnect wires remains one of the key design challenges for nanometer-scale VLSI designs. To enable fast evaluation of EM-induced damage, it is necessary to solve the partial differential equations (PDEs) governing stress evolution in confined metal interconnect trees, which is a time-consuming process. In this work, we propose two fast EM stress analysis techniques based on the *rational Krylov subspace reduction* techniques. Unlike traditional Krylov subspace method, which can be viewed as expansion around zero frequency (infinite time), rational Krylov subspace allows expansion at specific time constants, enabling better alignment with application-specific metrics such as nucleation time. As a result, very compact models can be achieved with almost zero error loss. We explore the rational Krylov subspace reduction via two simulation frameworks: one in frequency domain via extended rational Krylov subspace method termed *ExtRaKrylovEM*, and one in the time domain via rational Krylov exponential integration (EI) method termed *EiRaKrylovEM*. We show that the accuracy of both methods is sensitive to the selection of expansion point or shift time in this work. We further show that the good shift time typically is close to the time of interests such as nucleation time or steady-state time for the first time, which provides a good starting point to search the optimal shift time under a given reduction order. To further improve fidelity, we develop a coordinate descent optimization method that identifies the optimal reduction order and shift times for both nucleation and post-void phases. Experimental results on synthesized structures and industry designs demonstrate that *ExtRaKrylovEM* and *EiRaKrylovEM* achieve orders-of-magnitude improvements over the standard finite difference method in both efficiency and accuracy. Specifically, using only 4–6 reduction orders, our methods deliver sub-0.1% error in nucleation time and resistance change predictions while providing 20–500× speedup over finite-difference solution dependent on the number of simulation steps. In stark contrast, standard extended Krylov methods require 50+ orders yet still exhibit 10–20% nucleation time errors, rendering them impractical for EM-aware optimization and stochastic EM analysis.

Keywords: Electromigration, Rational Krylov Subspace, Exponential Integration, VLSI Reliability.

I. INTRODUCTION

Electromigration (EM) is a key reliability concern in VLSI interconnects, arising from the momentum transfer between high-current-carrying electrons and metal atoms. This atomic flux induces compressive stress near the anode and tensile stress near the cathode to generate back stress to counter the atomic flux. When the stress exceeds a critical threshold, voids or hillocks can form to relax the stress, leading to open or short failures.

This work is supported in part by NSF grants under No. CCF-2007135, and in part by NSF grant under No. CCF-2305437.

It was traditionally modeled using empirical formulas such as Black’s equation [1] and Blech’s product [2], which relate the mean time to failure (MTTF) of a wire segment to its current density and temperature. However, those empirical models have faced growing criticism for being overly conservative and only applicable to a single wire segment [3], [4]. To address these issues, several physics-based EM models and assessment techniques based on Korhonen’s equations [5] have recently been proposed [6], [7], [8], [9], [10], [11], [12], [13], [14], [15], [16], [17], [18], [19], [20], [19], [21].

Unlike traditional EM models that rely on current density in a single wire segment, physics-based EM models consider stress evolution across multiple wire segments in an interconnect tree, capturing complex interactions and correlations among them [22]. At the core of these approaches lies the numerical solution of Korhonen’s partial differential equation (PDE) for hydrostatic stress evolution under blocking boundary conditions [5]. While analytical approximations exist for limited structures [11], [23], general tree topologies require numerical methods such as finite difference, which become computationally expensive for large designs. To evaluate stochastic reliability metrics such as MTTF, Monte Carlo (MC) analysis is typically employed [24], [25], further amplifying the computational burden.

In this work, we address the computational challenges of physics-based EM analysis by accelerating the numerical solution of Korhonen’s equation through a novel *rational Krylov subspace scheme*. Unlike traditional Krylov methods that expand around zero frequency (infinite time), the rational Krylov subspace method allows expansion at specific time constants, enabling alignment with application metrics such as nucleation time in our context. This leads to highly compact models with minimal error. We exploit the rational Krylov subspace concept in two complementary simulation frameworks: frequency domain via the extended rational Krylov subspace method, and time domain via the rational Krylov exponential integration (EI) method. Our major contributions are as follows:

- First, we propose a novel *extended rational Krylov subspace* method, called *ExtRaKrylovEM*, that integrates the extended Krylov framework with the rational subspace concept to efficiently reduce the EM matrices derived from Korhonen’s equation in the frequency domain. The rational Krylov approach shifts the projection subspace toward critical time regions of interest in the stress evolution, such as the nucleation phase. This capability enables significantly higher accuracy with much smaller reduction orders compared to conventional extended Krylov

methods. *ExtRaKrylovEM* also naturally mitigates the singularity issue in the EM matrix inversion process.

- Second, we extend the rational Krylov subspace concept to the time domain through an exponential integration (EI) framework, yielding the *EiRaKrylovEM* method. This approach constructs a rational Krylov subspace to efficiently approximate the matrix exponential action on the initial stress vector, enabling accurate time-domain simulation of stress evolution with substantially reduced computational cost. By strategically selecting shift times aligned with critical phases of stress evolution, *EiRaKrylovEM* achieves significant speedups over conventional time-stepping methods while maintaining high accuracy.
- To determine the optimal reduction order and shift parameters for both nucleation and post-void phases, we develop a gradient descent-based optimization algorithm driven by application-specific metrics—namely, nucleation time (determined by critical stress thresholds) and resistance change in voided segments (also stress-dependent). This contrasts with existing rational Krylov methods that rely on generic frequency- or time-domain error based on all system dynamics. By directly optimizing for EM-relevant performance metrics, our approach yields reduced-order models that more accurately capture the critical stress dynamics governing interconnect reliability.
- Experimental results on a number of synthesized structures and industry designs (one ARM design and a number of IBM benchmarks) show that the proposed *ExtRaKrylovEM* and *EiRaKrylovEM* can achieve orders-of-magnitude improvements in both efficiency and accuracy. Specifically, using only 4–6 reduction orders, our methods deliver sub-0.1% error in nucleation time and resistance change predictions while providing 20–500× speedup over finite-difference solutions depending on the time steps of simulation. In stark contrast, the standard extended Krylov methods require 50+ orders yet still exhibit 10–20% nucleation time errors, rendering them impractical for EM-aware optimization and stochastic EM analysis.

The paper is organized as follows. In Section II, we review the related works on EM analysis and Krylov subspace methods. In Section III, we present the preliminaries of EM stress evolution modeling and introduce the concept of the rational Krylov subspace methods. In Section IV, we detail the proposed *ExtRaKrylovEM* method and also present the coordinate descent algorithm. In Section V, we describe the *EiRaKrylovEM* method. In Section VI, we present experimental results. Finally, we conclude the paper in Section VII.

II. REVIEW OF RELEVANT WORKS

Krylov subspace methods have been widely used for model order reduction in various domains [26], including VLSI circuit simulation [27]. Existing methods mainly focus on reducing models of large dynamic systems but are difficult to handle systems with large inputs and outputs. To mitigate this issue, the extended Krylov subspace method [28] and Krylov-based exponential integration (EI) frameworks [29] have been

proposed, which can naturally incorporate input excitations into the reduced model. The second issue with the existing Krylov subspace methods is that traditional Krylov methods typically expand the subspace around zero frequency (infinite time), which may not effectively capture the dynamics of interest in EM stress evolution.

For EM analysis, Krylov subspace methods have been applied to electromigration (EM) stress analysis in *FastEM*, where the extended Krylov subspace framework is implemented within a finite-difference formulation [30]. The standard Krylov approach can be interpreted as a subspace expansion around the frequency point $s = 0$ (corresponding to time $t \rightarrow \infty$). Consequently, it often requires a high reduction order to accurately capture transient behaviors such as the nucleation phase, which occurs far from the asymptotic regime. As shown in Fig. 1, the standard Krylov method exhibits significant deviation in predicting the nucleation time (critical stress of 10^3 Pa) even at order 50—the estimated nucleation time is about 8×10^4 s, compared to 4×10^4 s obtained by the Backward Euler reference. Moreover, the numerical error may lead to incorrect identification of the cathode nucleation node. In contrast, when using the extended Krylov subspace method with the shift time aligned to the nucleation time and order of 5 (e.g., $t_{\text{shift}} = 3.67 \times 10^4$ s), the results match the Backward Euler solution almost exactly.

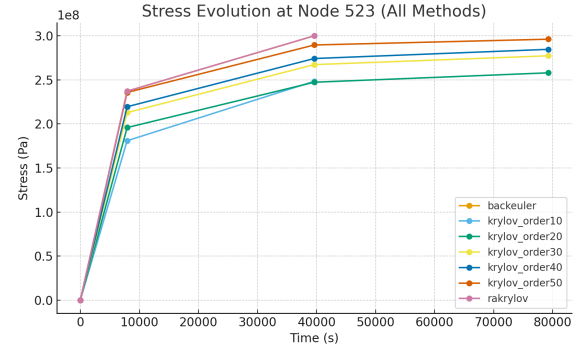


Fig. 1: The nucleation times at different reduction order using standard Krylov subspace method for a 100 segment wire (critical stress is 10^8 Pa)

Rational Krylov subspaces have been applied in a variety of numerical modeling contexts, including the solution of Maxwell's equations [31], VLSI power-grid analysis [32], and, more recently, EM stress analysis [33], all within the exponential integration (EI) framework. In the EI method, the Krylov subspace is used to approximate the matrix-exponential operation $e^{tA}\nu$ in the time domain, where t is the time variable and ν is the initial state vector. A fundamental limitation of this approach is that time-varying input sources require recomputation of the Krylov subspace at each change because the computed subspace only incorporates the input excitation from the previous time step, making EI methods inefficient for many practical analyses.

In the EM formulation of [33], a rational Krylov method is also employed; however, it constructs the Krylov subspace using $(A^{-1} - \sigma I)^{-1}$ rather than $(A - \sigma I)^{-1}$ as adopted in [32] and in our work, where A is the EM operator defined in Eq. (4). This choice biases the Krylov basis toward the dominant eigenvalues of A , thereby emphasizing high-

frequency (short-transient) dynamics. In electromigration analysis, however, the primary quantities of interest—nucleation time and post-void stress evolution—are governed by the smallest eigenvalues of A , which correspond to long-tail, near-steady-state behavior. As shown in [32], using A^{-1} (or its shifted variant) is preferable because the largest eigenvalues of A^{-1} correspond to the smallest eigenvalues of A , precisely the spectral components dominant in EM-induced failure mechanisms.

Furthermore, the method in [33] selects the shift time or expansion point and reduction order purely based on minimizing the global model residual error, rather than application-specific performance metrics such as nucleation time or resistance evolution. This often leads to unnecessarily high reduction orders that emphasize short transient effects rather than the long-tail dynamics relevant to EM-induced failure analysis.

In this work, we exploit the rational Krylov subspace method in two simulation frameworks: one in frequency domain via extended rational Krylov subspace method, and one in the time domain via rational Krylov exponential integration (EI) method. In the frequency-domain approach, we apply the rational Krylov subspace method to approximate the EM dynamic system directly in the frequency domain within a model-order reduction framework that naturally incorporates arbitrary input-current waveforms via the extended Krylov subspace. This formulation avoids the matrix-inversion singularity issues encountered in traditional finite difference methods during the nucleation phase [30]. In the time-domain approach, we develop a rational Krylov EI method that constructs the Krylov subspace using $(A - \sigma I)^{-1}$, enabling efficient approximation of the matrix exponential action on the initial stress vector while focusing on the low-frequency dynamics relevant to EM reliability assessment.

III. PRELIMINARIES

A. EM stress modeling in a nutshell

In confined metal wires subjected to high current densities, EM occurs as atoms are migrated from the cathode to the anode due to interactions between electrons and metal atoms [1]. Over time, this atom migration may potentially cause void and hillock formations that compromise interconnect functionality. Existing current-density based models such as Blech's limit [2] and Black's MTTF [1] consider only one wire segment at a time and those models are widely considered to be too conservative.

Recently physics-based EM modeling has been proposed, which boils down to solving Korhonen's equation for multi-segment interconnects in the same metallization connection tree [34]. The equation for the nucleation phase in multi-segment interconnects is given by Eq. (1),

$$\begin{aligned} PDE : \frac{\partial \sigma_{ij}(x, t)}{\partial t} &= \frac{\partial}{\partial x} \left[\kappa_{ij} \left(\frac{\partial \sigma_{ij}(x, t)}{\partial x} + G_{ij} \right) \right], \quad t > 0 \\ BC : \sigma_{ij1}(x_i, t) &= \sigma_{ij2}(x_i, t), \quad t > 0 \\ BC_{neu} : \sum_{ij} \kappa_{ij} \left(\frac{\partial \sigma_{ij}(x, t)}{\partial x} \right) &|_{x=x_{junc}} + G_{ij}, \quad t > 0 \\ BC_{neu} : \kappa_{ij} \left(\frac{\partial \sigma_{ij}(x, t)}{\partial x} \right) &|_{x=x_b} + G_{ij} = 0, \quad t > 0 \\ IC : \sigma_{ij}(x, 0) &= \sigma_{ij, T} \end{aligned} \quad (1)$$

here $\sigma_{ij}(x, t)$ represents the stress in the interconnect segment ij connecting nodes i and j . In Eq. (1), G_{ij} denotes the EM driving force in segment ij , calculated as $G_{ij} = \frac{e \rho J_{ij} Z^*}{\Omega}$, where J_{ij} is the current density in segment ij . The stress diffusivity κ_{ij} is defined by $\kappa_{ij} = D_a B \Omega / (k_B T)$, where D_a is the effective atomic diffusion coefficient, B is the effective bulk modulus, k_B is Boltzmann's constant, T is the absolute temperature, and E_a is the EM activation energy. e is the electron charge, ρ is resistivity, and Z^* is the effective charge.

The first BC in Eq. (1) enforces stress continuity at inter-segment junctions, specifically at $x = x_r$. The second BC, which is Neumann BC, addresses atomic flux conservation at inter-segment junction nodes x_{junc} , while the third Neumann BC applies to blocking natural terminal boundaries $x = x_b$, ensuring zero atomic flux. The IC specifies that the initial stress distribution in segment ij is given by $\sigma_{ij, T}$, which typically is zero.

In multi-segment interconnect trees, void nucleation occurs at the cathode when the steady-state nucleation stress surpasses the critical stress σ_{crit} . This moment marks the nucleation time, denoted as t_{nuc} . Beyond this time, $t > t_{nuc}$, the void grows larger and may lead to wire segment resistance changes. Once nucleated, the stress at the interface of the void dramatically drops to zero [35].

The new additional BCs describing the post-voiding phase are outlined in Eqs. (2) [8], which presume the $x = x_{nuc}$ node as the cathode where the void forms.

$$\begin{aligned} BC_{robin} : \frac{\partial \sigma(x_{nuc}, t)}{\partial x} &|_{x=x_{nuc}} = \frac{\sigma(0, t)}{\delta}, \quad t > 0 \\ BC_{neu} : \frac{\partial \sigma(0, t)}{\partial x} &|_{x=x_b} = -G, \quad t > 0 \\ IC : \sigma(x, 0) &= \sigma_{nuc}(x, t_{nuc}), \quad t = 0 \end{aligned} \quad (2)$$

where δ is the effective thickness of the void, which is quite small in general. As a result, the Robin BC $\frac{\partial \sigma(x_{nuc}, t)}{\partial x} |_{x=x_{nuc}} = \frac{\sigma(x_{nuc}, t)}{\delta}$ will generate a strong force to reduce the stress at location x_{nuc} until it becomes zero (atomic flux also becomes zero as well) in a very short period of time. Also the stresses in all the wire segments eventually become negative in steady-state (becomes compressive stress). Fig. 2 shows the stress evolution in 4 segments (out of 5 segment wires). The void is nucleated at segment 5's terminal (with critical stress $= 3 \times 10^8$ Pa). Almost immediately, the terminal's stress becomes zero after nucleation.

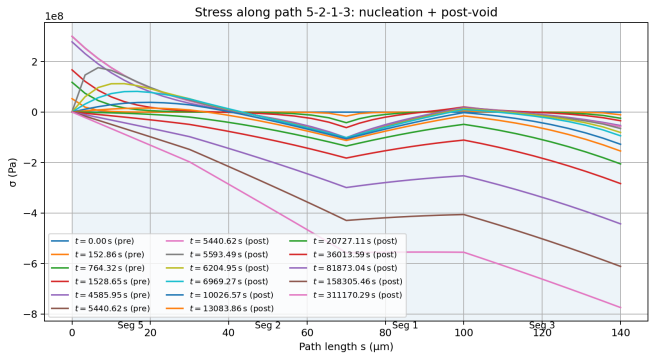


Fig. 2: The stress evolution in 4 segments of 5-segment wire including nucleation and post-void phases

B. Finite difference method for solving EM PDE

By using finite difference method, one can discretize Eq. (1) uniformly by splitting each segment into points with equal spacing Δx . Approximating the spatial derivative by its finite difference, for each discretized point i we obtain:

$$\frac{\partial \sigma}{\partial t} = \kappa \frac{\partial^2 \sigma}{\partial x^2} = \frac{(\sigma_{i+1} - 2\sigma_i - \sigma_{i-1})}{\Delta x^2}. \quad (3)$$

for all the internal nodes.

Applying finite-difference discretization to a k -segment interconnect wire yields n discrete nodes, which represent different topological locations along the wire tree: such as natural boundaries (including via connections), inter-segment points, inter-segment junctions. Incorporating the boundary conditions specified in Eq. (1) results in the following system of linear ordinary differential equations:

$$C\dot{\sigma}(t) = A\sigma(t) + B\mathbf{j}(t), \quad (4)$$

which governs the evolution of electromigration-induced stress within each interconnect segment and can be formulated as a linear time-invariant (LTI) system. Once the stress reaches the critical stress, a void will be nucleated at the cathode node of the wire segment. The void volume $V_v(t)$ in a multi-segment interconnect is governed by atom conservation, relating hydrostatic stress to the amount of depleted material [34]:

$$V_v(t) = - \int_{\Omega_L} \frac{\sigma(t)}{B} dV, \quad (5)$$

where Ω_L is the remaining wire domain, $\sigma(t)$ is the hydrostatic stress field, and B is the (effective) bulk modulus of the metal. Once the void exceeds the critical size (such as the width of the wire), current is partially diverted through the barrier, and the wire resistance increases, which can be approximated as

$$\Delta R(t) = \frac{V_v(t) - V_{\text{crit}}}{WH} \left[\frac{\rho_{\text{Ta}}}{h_{\text{Ta}}(2H + W)} - \frac{\rho_{\text{Cu}}}{HW} \right], \quad t_{\text{inc}} < t, \quad (6)$$

where W and H are the copper line width and thickness, ρ_{Ta} and ρ_{Cu} are the resistivities of barrier (e.g., Ta/TaN) and Cu, and h_{Ta} is the barrier thickness. Here V_{crit} denotes the critical void volume (or an equivalent critical cross-section length in 1D).

C. Overview of the Rational Krylov Subspace Method

The classical Krylov subspace method constructs an orthonormal basis $\mathcal{K}_q(G, b) = \text{span}\{b, Gb, G^2b, \dots, G^{q-1}b\}$ for the system matrix $G = A^{-1}$, where A is an $n \times n$ coefficient matrix from the LTI system $\dot{x}(t) = Ax(t) + Bu(t)$ and $b = -A^{-1}B$ is the excitation vector derived from the input waveform, and B is a $n \times m$ input matrix. While this standard Krylov basis tries to capture the largest or dominant eigenvalues of A , around the expansion point $s = 0$ or $t = \infty$, its accuracy deteriorates for systems whose important dynamics occur at earlier times or lower frequencies.

To overcome this limitation, the *rational* Krylov subspace introduces a complex shift (or pole) $\sigma \in \mathbb{C}$ and forms the subspace

$$\mathcal{K}_q((A - \sigma I)^{-1}, (A - \sigma I)^{-1}B) = \text{span}\{v_1, (A - \sigma I)^{-1}v_1, \dots, ((A - \sigma I)^{-1})^{q-1}v_1\}. \quad (7)$$

where $v_1 = (A - \sigma I)^{-1}B$.

Let $V_m = [v_1, \dots, v_q] \in \mathbb{R}^{n \times (qxm)}$ be the orthonormal basis of this subspace. The rational Arnoldi decomposition is given by:

$$(A - \sigma I)^{-1}V_q = V_q H_q + h_{q+1,q} v_{q+1} e_q^\top, \quad (8)$$

where $H_m \in \mathbb{R}^{q \times q}$ is an upper Hessenberg matrix and $e_q^\top = [0, \dots, 0, 1]$.

By shifting the system matrix with $(A - \sigma I)$, the resulting basis better aligns with the spectral region (related eigenvalues) corresponding to the time window or frequency range of interest (e.g., around the nucleation time in EM-stress evolution). The rational Krylov process thus enables accurate approximation computing or reduced-order models with significantly smaller dimensions, as the choice of σ allows the projection space to focus on the most *relevant* poles of the system. The final reduced matrices are obtained by congruence transformation: $A_h = V_q^T A V_q$ and $B_h = V_q^T B$ where V_q contains the orthonormal basis vectors generated by the rational Arnoldi process. This framework generalizes the standard Krylov approach and serves as the foundation for our proposed extended rational Krylov reduction method for fast EM analysis.

IV. THE NEW STRESS ANALYSIS BASED ON EXTENDED RATIONAL KRYLOV SUBSPACE METHOD

A. The proposed Extended Rational Krylov EM Analysis

After spatial discretization of the electromigration (EM) stress equation, the resulting linear time-invariant (LTI) system can be written as

$$\dot{x}(t) = Ax(t) + Bu(t), \quad x(0) = [x_1(0), x_2(0), \dots, x_n(0)]^T, \quad (9)$$

where $x(t)$ denotes the nodal stress vector and $j(t)$ is the piecewise constant current-density. The current input can be represented as

$$u(t) = u_1(t) + u_2(t - t_1) + u_3(t - t_2) + \dots + u_N(t - t_{N-1}). \quad (10)$$

Applying the Laplace transform to Eq. (9) yields

$$sCX(s) - Cx(0) = AX(s) + \frac{1}{s}BJ_1, \quad (11)$$

where the transformed input is

$$J(s) = \frac{1}{s} \sum_{i=1}^N u_i e^{t_{i-1}} = \frac{1}{s} J_1. \quad (12)$$

Note that the input can be any other forms like piecewise linear (PWL). In case of PWL, $J(s)$ will be $\frac{1}{s^2} J_1$ format.

In the standard extended Krylov subspace method, the expansion is centered at $s = 0$, which effectively captures very low-frequency (steady-state) behavior. To enhance accuracy at finite time scales, we perform the expansion around a shifted frequency $s = \sigma$, where σ is selected to match the time region of interest (e.g., the nucleation time). Substituting $s = \sigma + \Delta s$ into Eq. (11) yields

$$(\sigma + \Delta s)X(\sigma + \Delta s) - x(0) = AX(\sigma + \Delta s) + \frac{1}{\sigma + \Delta s}BJ_1. \quad (13)$$

Define $\tilde{X}(\Delta s) = (\sigma + \Delta s)X(\sigma + \Delta s)$ and expand it in a Taylor series about $\Delta s = 0$:

$$(\sigma + \Delta s)(m_0 + m_1\Delta s + m_2\Delta s^2 + \dots) - (\sigma + \Delta s)x(0) = A(m_0 + m_1\Delta s + m_2\Delta s^2 + \dots) + BJ. \quad (14)$$

Matching terms of equal powers of Δs yields the recursive moment equations:

$$\begin{aligned} m_0 &= -(A - \sigma I)^{-1}BJ_1, \\ m_1 &= (A - \sigma I)^{-1}(m_0 - x(0)), \\ m_2 &= (A - \sigma I)^{-1}m_1, \\ &\vdots \\ m_{q-1} &= (A - \sigma I)^{-1}m_{q-2}. \end{aligned} \quad (15)$$

Instead of directly forming the raw moments in Eq. (15), an orthonormal rational Krylov basis is constructed using the modified Arnoldi process. Define

$$G_\sigma = (A - \sigma I)^{-1}, \quad b_\sigma = -(A - \sigma I)^{-1}BJ_1, \quad (16)$$

then the rational Krylov subspace is

$$\mathcal{K}_q(G_\sigma, b_\sigma) = \text{span}\{b_\sigma, G_\sigma b_\sigma, G_\sigma^2 b_\sigma, \dots, G_\sigma^{q-1} b_\sigma\}. \quad (17)$$

This subspace effectively aligns the reduced-order model with the dominant dynamics governed by σ , achieving higher transient accuracy with much smaller reduction orders.

Using the projection matrix V_q formed by the orthonormal basis vectors, the reduced matrices are obtained as

$$\hat{A} = V_q^T A V_q, \quad \hat{B} = V_q^T B, \quad \hat{x}(0) = V_q^T x(0). \quad (18)$$

The reduced LTI system becomes

$$\dot{\hat{x}}(t) = \hat{A} \hat{x}(t) + \hat{B} J_1, \quad \hat{x}(0) = [\hat{x}_1(0), \dots, \hat{x}_q(0)]^T. \quad (19)$$

Time-domain integration of Eq. (19) is carried out using the backward-Euler method, and the full-space stress field is recovered as

$$x(t) = V_q \hat{x}(t). \quad (20)$$

Note that since we compute or solve for $(A - \sigma I)^{-1}$, which is typically full rank (unless σ is an eigenvalue of A) instead of A^{-1} , we automatically mitigate the singularity issue of A matrix reported [36], [13]. The resulting extended rational Arnoldi process is illustrated in Algorithm 1 where $C = I$ in our case.

B. Selection of reduction order and shift time

One critical aspect of the rational Krylov subspace method is to select the shift frequency σ . In this work, instead of using σ , we chose to use shift time $t_s = 1/\sigma$, which can be viewed as the time constant of the system that we are more interested in.

Algorithm 1 Extended Rational Arnoldi Algorithm

Input: System matrices A, B, C , input vector u , rational shift σ , optional initial stress x_0 , and reduction order q
Output: Reduced matrices A_h, B_h, C_h , projection matrix V , and upper Hessenberg matrix H

- 1: Factorize the shifted matrix: $(A - \sigma I) = LU$
- 2: Define the inverse operator $\mathcal{A}^{-1}v = (A - \sigma I)^{-1}v$
- 3: Compute $r_1 = -\mathcal{A}^{-1}(Bu)$
- 4: Normalize $v_1 = r_1/\|r_1\|$, set $V = [v_1]$
- 5: **if** $\sigma_0 \neq 0$ **then**
- 6: $r_2 = \mathcal{A}^{-1}(C(v_1 - x_0))$
- 7: **else**
- 8: $r_2 = \mathcal{A}^{-1}(Cv_1)$
- 9: **end if**
- 10: Orthogonalize: $r_2 = r_2 - (v_1^T r_2)v_1$, normalize $v_2 = r_2/\|r_2\|$
- 11: Append v_2 to V
- 12: **for** $j = 3$ to q **do**
- 13: $w = \mathcal{A}^{-1}(v_{j-1})$
- 14: **for** $i = 1$ to $j-1$ **do**
- 15: $h_{ij} = v_i^T w$
- 16: $w = w - h_{ij}v_i$
- 17: **end for**
- 18: $\beta = \|w\|$
- 19: **if** $\beta < \varepsilon$ **then break**
- 20: **end if**
- 21: $v_j = w/\beta$
- 22: Append v_j to V
- 23: **end for**
- 24: Form reduced matrices:

$$A_h = V^T A V, \quad B_h = V^T B, \quad C_h = V^T C V$$

25: **return** (A_h, B_h, C_h, V, H)

C. Initial estimation of shift time for nucleation phase and post-void phase

To estimate the initial shift time for nucleation phase, we can use the analytical solution of 1D diffusion equation as a reference. The 1D diffusion equation is given as

$$\frac{\partial \sigma(x, t)}{\partial t} = \kappa \frac{\partial^2 \sigma(x, t)}{\partial x^2} \quad (21)$$

where $\sigma(x, t)$ is the hydrostatic stress and κ is the effective stress diffusivity. For a given wire segment of length L under atomic blocking conditions at both ends, the system has the following eigenvalues:

$$\lambda_n = \left(\frac{n\pi}{L}\right)^2, \quad n = 1, 2, \dots \quad (22)$$

By using the slowest decaying mode where $n = 1$, $\lambda_1 = \left(\frac{\pi}{L}\right)^2$. So the slowest exponential decay is: $\exp\left(-\kappa \frac{\pi^2}{L^2} t\right)$ therefore the shift time can be estimated as

$$\tau = \frac{L^2}{\pi^2 \kappa} \quad (23)$$

In this work, we employ the average wire segment length L_{avg} to establish the nucleation estimation base τ_{nuc} , and use the longest distance L_{max} between any two points in the tree structure to define the post-void time estimation base τ_{post} . This choice is motivated by the distinct physics governing each phase: nucleation time is predominantly influenced by local stress gradients within individual wire segments under

electron wind forcing, making it sensitive to the characteristic segment length. In contrast, post-void resistance evolution is governed by void propagation along the critical path of the interconnect tree, rendering it sensitive to the maximum path length where atom depletion occurs. This dual-scale approach ensures that the shift times accurately reflect the dominant time constants in each regime of EM degradation. For nucleation time shift, we can also use the analytic nucleation time formula for a single wire segment [37]. Since those shift time is just initial estimation, either way is acceptable.

In this work, we use (23), with L_{avg} for nucleation phase and L_{max} for post-void phase as the basis to find the best shift time for both phases as shown in the next subsection.

D. Coordinate Descent Algorithm for Order and Shift Time Selection

In this subsection, we present a coordinate descent strategy with multi-scale line search to tune the Krylov order and shift parameters. The optimization focuses on the reduction order and shift times for both nucleation and post-void phases in the rational Krylov EM analysis. The goal is to identify the optimal configuration that minimizes the combined percentage error in nucleation time and resistance change within the specified parameter search ranges, while maintaining the reduction order as low as possible to ensure computational efficiency.

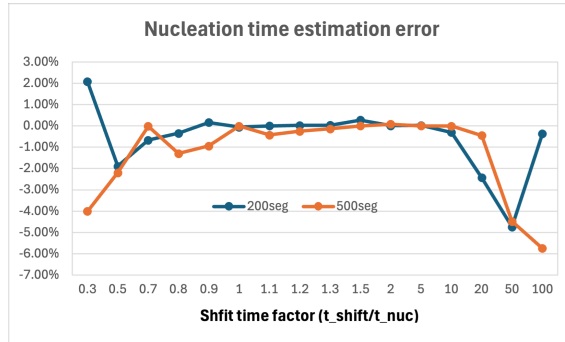


Fig. 3: The calculated nucleation time vs shift time used (critical stress is 10^8 Pa)

In the coordinate descent algorithm, we look at nucleation time t_{nuc} and nucleated wire segment resistance change ΔR as performance metrics and compute their percentage changes with respect to the reference results. We change the parameters one at a time to avoid computing gradients of the objectives directly. It is suitable for the optimization problem with small number of parameters and limited search space as we have.

Furthermore, instead of using shift time directly, we use shift time scaling factors η_{nuc} and η_{post} to scale the estimated shift times for nucleation and post-void phases, respectively. For instance, $\eta_{\text{nuc}} = 1$ means that the estimated shift time for nucleation phase is $1 \times \tau_{\text{nuc}}$, while other values scale it accordingly. Similarly, η_{post} scales the shift time for the post-void phase.

Next, we determine the search ranges for these parameters. Fig. 3 illustrates the nucleation time estimation errors obtained by the ExtRaKrylov method across different shift time factors η_{nuc} ranging from 0.3 to 100. As we can see that when η_{nuc} lies between 0.7 and 10, the results exhibit high accuracy (less than 0.01% error on average). In practice, setting $\eta_{\text{nuc}} = 1$

typically achieves less than 1% error with order 4 or 5. Similar behavior is observed for post-void phase resistance change estimation. Nevertheless, we develop a coordinate descent method to systematically identify the optimal combination of order and shift time for both nucleation and post-void phases.

Based on these observations, we set the candidate order set or range to $\mathcal{M} = \{3, 4, 5, 6\}$, since orders within this range typically provide sufficient accuracy. For the shift time scaling factors η_{nuc} and η_{post} , we set their search ranges to $[0.1, 20]$, as shift times outside this range yield poor accuracy as shown in Fig. 3.

Algorithm 2 summarizes the proposed coordinate-descent approach for tuning rational Krylov parameters in EM analysis. The algorithm seeks to minimize a combined objective function J that captures both nucleation time and resistance change errors. This algorithm will be applied to the *EiRaKrylovEM* solvers (to be discussed later) for nucleation and post-void phases as well. We define the percentage error (PE) as

$$\text{PE}(x, y) \triangleq 100 \frac{|x - y|}{|x| + \epsilon}, \quad (24)$$

where ϵ is a small regularization constant to avoid division by zero. The combined objective function is then given by

$$\begin{aligned} J(q, \eta_{\text{nuc}}, \eta_{\text{post}}) \triangleq & \text{PE}(t_{\text{nuc}}^{\text{ref}}, t_{\text{nuc}}(q, \eta_{\text{nuc}})) \\ & + \text{PE}(\Delta R^{\text{ref}}, \Delta R(q, \eta_{\text{post}})), \end{aligned} \quad (25)$$

where $t_{\text{nuc}}^{\text{ref}}$ and ΔR^{ref} denote reference values from high-fidelity simulations, while $t_{\text{nuc}}(q, \eta_{\text{nuc}})$ and $\Delta R(q, \eta_{\text{post}})$ represent the reduced-order predictions for nucleation time and resistance change, respectively.

The main routine performs coordinate descent to optimize the reduction order q and the shift-time scaling factors η_{nuc} and η_{post} . The algorithm iteratively refines these parameters by alternating discrete searches over the candidate order set \mathcal{M} and does step-based search for the shift factors within their bounds $[\eta_{\text{min}}, \eta_{\text{max}}]$. Iterations continue until the improvement in J falls below a threshold τ_{stop} or the maximum number of iterations is reached. The optimized parameters $(q^*, \eta_{\text{nuc}}^*, \eta_{\text{post}}^*)$ and the corresponding minimal objective J^* are then used in the rational Krylov EM solvers.

V. NEW EXPONENTIAL INTEGRATION STRESS ANALYSIS BASED ON RATIONAL KRYLOV METHODS

In this section, we present the new exponential integration method based on rational Krylov methods, called *EiRaKrylovEM*

We first review the exponential integration framework for solving linear ODEs, followed by the rational Krylov subspace approximation of the matrix exponential operator. We then present the residual error estimation. We first re-write linear ordinary differential equation from (4) as follows:

$$\frac{d\sigma(t)}{dt} = A\sigma(t) + b, \quad b = B u, \quad (26)$$

assuming that with constant input u (for the time being) and initial condition $\sigma(0) = \sigma_0$. Let's further define

$$f = A^{-1}b, \quad v_0 = \sigma_0 + f. \quad (27)$$

Algorithm 2 Coordinate Descent Method For Shift Time and Order Selection

Input: candidate order set \mathcal{M} , shift-factor bounds $[\eta_{\min}, \eta_{\max}]$
Output: Best parameters $(q^*, \eta_{\text{nuc}}^*, \eta_{\text{post}}^*)$ and best J^*

Initialization

- 1: Choose initial $(q, \eta_{\text{nuc}}, \eta_{\text{post}})$, $J^* \leftarrow J(q, \eta_{\text{nuc}}, \eta_{\text{post}})$
- 2: Set step-size list \mathcal{S} (coarse-to-fine)

Coordinate Descent Loop

- 3: **for** $iter = 1$ to I_{\max} **do**
- 4: $J_{\text{prev}} \leftarrow J^*$
- 5: (1) *Optimize order q over \mathcal{M}*
 - 6: **for** each $q_c \in \mathcal{M}$ **do**
 - 7: $J_c \leftarrow J(q_c, \eta_{\text{nuc}}, \eta_{\text{post}})$
 - 8: **if** $J_c < J^*$ **then** $(q, J^*) \leftarrow (q_c, J_c)$
 - 9: **end if**
 - 10: **end for**
 - 11: (2) *Optimize η_{nuc} via step search*
 - 12: **for** each $s \in \mathcal{S}$, $d \in \{+1, -1\}$ **do**
 - 13: $\eta_c \leftarrow \text{clip}(\eta_{\text{nuc}} + d s, \eta_{\min}, \eta_{\max})$
 - 14: **if** $J(q, \eta_c, \eta_{\text{post}}) < J^*$ **then** $(\eta_{\text{nuc}}, J^*) \leftarrow (\eta_c, J(q, \eta_c, \eta_{\text{post}}))$; **Break**
 - 15: **end if**
 - 16: **end for**
 - 17: (3) *Optimize η_{post} via step search*
 - 18: **for** each $s \in \mathcal{S}$, $d \in \{+1, -1\}$ **do**
 - 19: $\eta_c \leftarrow \text{clip}(\eta_{\text{post}} + d s, \eta_{\min}, \eta_{\max})$
 - 20: **if** $J(q, \eta_{\text{nuc}}, \eta_c) < J^*$ **then** $(\eta_{\text{post}}, J^*) \leftarrow (\eta_c, J(q, \eta_{\text{nuc}}, \eta_c))$; **Break**
 - 21: **end if**
 - 22: **end for**
 - 23: **if** $J_{\text{prev}} - J^* < \tau_{\text{stop}}$ **then Break**
 - 24: **end if**
 - 25: **end for**
 - 26: **return** $(q, \eta_{\text{nuc}}, \eta_{\text{post}}, J^*)$

The closed-form solution for (4) is

$$\sigma(t) = e^{tA}(\sigma_0 + A^{-1}b) - A^{-1}b. \quad (28)$$

$$= e^{tA}v_0 - f \quad (29)$$

Computing the matrix exponential $e^{tA}v_0$ is generally very expensive. The key idea of the EI based method is to approximate it using a rational Krylov subspace method.

A. Rational Krylov Approximation for the Matrix Exponential

Specifically, the key computing step is to approximate $e^{tA}v_0$ in (29) using a rational Krylov subspace method. There are several Krylov subspaces we can select, such as standard $\mathcal{K}_q(A, v_0)$, inverse $\mathcal{K}_q(A^{-1}, v_0)$, and rational Krylov subspaces $\mathcal{K}_q((A - \sigma I)^{-1}, v_0)$ [29].

It was shown that the rational Krylov subspace can provide much better approximation than the standard and inverse Krylov subspaces in EI framework for IR drop analysis [32]. However, the shift or expansion point σ in this method does not correlate well to the accuracy of the circuit analyzed. We further note that the work in [33] used

$\mathcal{K}_q((A^{-1} - \sigma I)^{-1}, v_0)$, instead of typical rational Krylov subspace $\mathcal{K}_q((A - \sigma I)^{-1}, v_0)$.

In this paper, we show that the standard rational Krylov subspace $\mathcal{K}_q((A - \sigma I)^{-1}, v_0)$ turns out to be a good choice for the EM stress analysis problem as the shift σ can be aligned with the time of interest such as nucleation time or steady state time, which are wire and application specific for EM analysis.

For rational Krylov subspace $\mathcal{K}_q((A - \sigma I)^{-1}, v_0)$, let H_m denote the resulting reduced (square) Hessenberg matrix. Let $V_m = [v_1, \dots, v_q]$ orthogonal basis of the rational Krylov subspace, which satisfies the Arnoldi decomposition (8). Then the mapped reduced operator is defined as

$$\hat{H}_q = H_q^{-1} + \sigma I_q, \quad (30)$$

which corresponds to the identity

$$A = \sigma I + ((A - \sigma I)^{-1})^{-1} \quad (31)$$

in the reduced space. Let $V_q \in \mathbb{R}^{n \times q}$ be the Krylov basis, $\beta = \|v_0\|_2$, and $e_1 = [1, 0, \dots, 0]^T \in \mathbb{R}^q$. The exponential integration (EI) approximation is given by [29]:

$$e^{tA}v_0 \approx \beta V_q e^{t\hat{H}_q} e_1. \quad (32)$$

Algorithm 3 constructs a rational Krylov subspace using repeated applications of $(A - \sigma I)^{-1}$ and returns the reduced Hessenberg matrix. It returns not only the V_q , H_q , but also $\beta, h_{k+1,k}, v_{k+1}$, which will be used for residual error computation later. Notice that $q = k$ if the process can finish to the order of q .

After the \hat{H}_q is calculated in (30), then the stress at time t can be computed

$$\sigma_q(t) = \beta V_q e^{t\hat{H}_q} e_1 - f. \quad (33)$$

For $t = 0$, the initial condition $\sigma(0) = \sigma_0$ is applied explicitly. The whole time domain analysis based on EI with rational Krylov subspace is summarized in Algorithm 4.

B. Residual Error Estimation

One important advantage of EI-Krylov based method is that we can estimate the residual errors in the time domain. Let the reduced state be

$$z_q(t) = e^{t\hat{H}_q} e_1. \quad (34)$$

The residual vector is approximated as [29]

$$r_q(t) \approx \beta (h_{q+1,q}, z_m(t)) v_{q+1}. \quad (35)$$

here (a, b) means inner product. Then, the absolute norm is

$$\|r_q(t)\|_2 = \|\beta (h_{q+1,:}, z_q(t)) v_{q+1}\|_2, \quad (36)$$

and the relative residual error is defined as

$$r_{\text{rel}}(t) = \frac{\|r_m(t)\|_2}{\max(\|\sigma_m(t)\|_2, 10^{-30})}. \quad (37)$$

For *EiRaKrylovEM* method, we can use the residual error estimation for error estimation in result section and to guide the selection of reduction order and shift time for both nucleation and post-void phases.

To find the best reduction order, shift time for nucleation and post-void phases, we again apply the coordinate descent

Algorithm 3 Rational Krylov Subspace Reduction With Residual Information

Input: Matrix $A \in \mathbb{R}^{n \times n}$, Vector $v \in \mathbb{R}^n$, Maximum Krylov Dimension q , Shift σ
Output: Basis $V_m = [v_1, \dots, v_k]$, Hessenberg Matrix $H_m \in \mathbb{R}^{k \times k}$, $\beta = \|v\|_2$, Last-Row Coefficients $h_{k+1,k}$, Next Basis Vector v_{k+1}

- 1: $\beta \leftarrow \|v\|_2$ and $v_1 \leftarrow v/\beta$
- 2: $V(:, 1) \leftarrow v_1$
- 3: Form $M \leftarrow A - \sigma I$
- 4: Compute LU Factorization $M = LU$
- 5: $k \leftarrow 0$ and $v_{k+1} \leftarrow \emptyset$
- 6: **for** $j = 1$ to q **do**
- 7: Solve $w \leftarrow M^{-1}V(:, j)$ Using LU Factors
- 8: **for** $i = 1$ to j **do**
- 9: $h_{i,j} \leftarrow V(:, i)^T w$
- 10: $w \leftarrow w - h_{i,j}V(:, i)$
- 11: **end for**
- 12: $h_{j+1,j} \leftarrow \|w\|_2$
- 13: **if** $h_{j+1,j} < \varepsilon$ **then**
- 14: $k \leftarrow j$
- 15: $v_{k+1} \leftarrow \emptyset$ ▷ Happy breakdown
- 16: **Break**
- 17: **end if**
- 18: $V(:, j+1) \leftarrow w/h_{j+1,j}$
- 19: $v_{k+1} \leftarrow V(:, j+1)$
- 20: $k \leftarrow j$
- 21: **end for**
- 22: $V_q \leftarrow V(:, 1:k)$
- 23: $H_q \leftarrow H(1:k, 1:k)$
- 24: $h_{k+1,k} \leftarrow H(k+1, 1:k)$
- 25: **return** $V_q, H_q, \beta, h_{k+1,k}, v_{k+1}$

algorithm Algorithm 2 presented in the previous section to minimize the combined error metric based on the nucleation time and the resistance change of the nucleated wire segment.

Note that in the previous discussions that we assume the input currents are constant during the entire simulation time. However, this is one major drawback of *EiRaKrylovEM* method or EI-related simulation method compared with frequency-domain *ExtRaKrylovEM*. If currents become time-varying [38], the Krylov subspace has to be rebuilt for each time step in which current changes, which will significantly diminish the efficiency advantage of the method.

VI. EXPERIMENTAL RESULTS

A. Experimental Setup

Our numerical experiments are conducted on an iMAC with an Apple M3 chip (8-core CPU and 32GB memory).

The proposed *ExtRaKrylovEM* and *EiRaKrylovEM* framework are fully developed using Python v3.11. We also implemented FastEM [13] and use the code from [18] as the FDM solver, which is the baseline for accuracy and performance comparison. To assess the accuracy and efficiency of *ExtRaKrylovEM* and *EiRaKrylovEM* solvers, we evaluate them on two categories of power-grid designs. (1) Synthetic multi-segment trees: We generate trees containing 100, 200, 500,

Algorithm 4 Exponential Integration Using Single-Shift Rational Krylov

Input: $\mathbf{A}, \mathbf{B}, \mathbf{u}, \sigma_0, \{t_k\}, q, \sigma$
Output: Stress trajectory $\{\sigma_q(t_k)\}$

- 1: $\mathbf{b} \leftarrow \mathbf{B}\mathbf{u}$
- 2: $\mathbf{f} \leftarrow \mathbf{A}^{-1}\mathbf{b}$
- 3: $\mathbf{v}_0 \leftarrow \sigma_0 + \mathbf{f}$
- 4: $\beta \leftarrow \|\mathbf{v}_0\|_2$
- 5: Construct rational Krylov basis $\mathbf{V}_q, \mathbf{H}_q, \mathbf{v}_{q+1}, \mathbf{h}_{q+1,1:q}$ using $(\mathbf{A} - \sigma\mathbf{I})^{-1}$
- 6: $\widehat{\mathbf{H}}_q \leftarrow \mathbf{H}_q^{-1} + \sigma\mathbf{I}$
- 7: **for** each t_k **do**
- 8: **if** $t_k = 0$ **then**
- 9: $\sigma_q(t_k) \leftarrow \sigma_0$
- 10: **else**
- 11: $\mathbf{z} \leftarrow e^{t_k \widehat{\mathbf{H}}_q} \mathbf{e}_1$
- 12: $\sigma_q(t_k) \leftarrow \beta \mathbf{V}_q \mathbf{z} - \mathbf{f}$
- 13: Compute residual using (36) and (37)
- 14: **end if**
- 15: **end for**
- 16: **return** $\{\sigma_q(t_k)\}$

1000, and 2000 segments with random geometries and current densities, following the multi-segment interconnect tree generation algorithm in [39] to cover designs with different sizes. These cases emulate practical power-grid structures with varying complexity, including segment geometry and current density. (2) Real design benchmarks: To further demonstrate the practicality of our method, we extract the three longest interconnect trees from the power grids of industrial designs, including ARM-Cortex [40] and IBM Power Grid Benchmarks [41] considering the higher EM vulnerability of long trees. These circuits are synthesized with 32nm technology. The accuracy of stress prediction and nucleation-time t_{nuc} estimation are used to evaluate the fidelity of our proposed methods, while the total runtime is reported to demonstrate the improvement on efficiency over prior work [18].

B. The sensitivity analysis for different configurations

First, we perform a simple sensitivity analysis to see how the model order q and shift factors $\{\eta_{\text{nuc}}, \eta_{\text{post}}\}$ affect the accuracy of the proposed methods.

We conduct a case study on a synthesized 500-segment interconnect tree representative of a typical block-level power grid. Table I summarizes the accuracy of the proposed sensitivity analysis across different model orders for the synthesized 500-segment interconnect tree.

We perform one time sweep over a set of candidate shift values s_f to identify the optimal configuration of model order q and shift factors $\{\eta_{\text{nuc}}, \eta_{\text{post}}\}$ that minimize the analysis error for both nucleation time and resistance change. As shown in the Table Ia, the sensitivity analysis identifies the optimal configuration $\{q^* = 5, \eta_{\text{nuc}}^* = 0.2, \eta_{\text{post}}^* = 3.5\}$, which reduces the analysis error to below 0.00% for both nucleation time and resistance change. In contrast, the baseline solver without sensitivity correction exhibits an error exceeding -13.6% for nucleation time.

TABLE I: Sensitivity Analysis results for our proposed (a) *ExtRaKrylovEM* and (b) *EiRaKrylovEM* on the 500-segment wire

(a) <i>ExtRaKrylovEM</i>									
Model Order q	$q = 3$		$q = 4$		$q = 5$		$q = 6$		
Phase	η_{Nuc}	η_{Post}	η_{Nuc}	η_{Post}	η_{Nuc}	η_{Post}	η_{Nuc}	η_{Post}	
s_f	15.5	0.6	3.5	20	0.2	3.5	0.2	4	
Error ϵ	0.06%	0.00%	0.01%	0.00%	0.00%	0.00%	0.00%	0.00%	

(b) <i>EiRaKrylovEM</i>									
Model Order q	$q = 3$		$q = 4$		$q = 5$		$q = 6$		
Phase	η_{Nuc}	η_{Post}	η_{Nuc}	η_{Post}	η_{Nuc}	η_{Post}	η_{Nuc}	η_{Post}	
s_f	0.3	20	6.5	19.5	0.1	18.5	0.4	0.8	
Error ϵ	1.11%	0.02%	0.02%	0.00%	0.03%	0.00%	0.01%	0.00%	

C. Accuracy and Performance of *ExtRaKrylovEM* and *EiRaKrylovEM* for Deterministic Analysis

To assess the accuracy and computational efficiency of the proposed *ExtRaKrylovEM* and *EiRaKrylovEM* methods relative to existing approaches, Table II and Table III report performance comparisons across a set of wire benchmarks. The evaluated methods include our *ExtRaKrylovEM*, the finite-difference (FDM) solver [18], and the Krylov-based FastEM framework [13].

For consistency, we set the critical stress threshold to $\sigma_{\text{crit}} = 10^8$ Pa for all analyses. For the standard Krylov-based FastEM method, we use a reduction order of 50 to ensure a fair comparison, as our methods also employ a nearly fixed order (4–6). Table II summarizes the performance comparison among the proposed *ExtRaKrylovEM*, the FDM solver [18], and FastEM [30] using 100 simulation time steps.

From Table II, we observe that the proposed *ExtRaKrylovEM* achieves approximately 34–189 \times speedup (80 \times on average) over the FDM-based solver for 100 time steps. The speedup also scales with the number of required time steps, as further illustrated in Fig. 4.

While *ExtRaKrylovEM* delivers only about 2.3 \times speedup compared to FastEM, the key distinction lies in accuracy. FastEM exhibits significant errors in nucleation time estimation, whereas our method attains near-zero error (less than 0.1% on average). As demonstrated in the motivating example (Section II), such errors can lead to incorrect nucleation location (cathode node) detection, which is unacceptable for reliable EM analysis. Consequently, a meaningful speedup comparison is only applicable against the FDM method, which serves as our accuracy baseline.

We also notice that all the methods give very good estimation on resistance change with almost zero errors. This is because the resistance change is mainly determined by the void size in the steady state, which is at the very long time scale where both standard Krylov (which is expanded at infinite time) and rational Krylov subspace can give good accuracy.

Table III presents the performance comparison between the proposed *EiRaKrylovEM* and the FDM solver [18] using 100 simulation time steps. As shown, *EiRaKrylovEM* achieves approximately 18–122 \times acceleration (50 \times on average) over FDM while maintaining similar accuracy with sub-0.1% error in both nucleation time and resistance change. Overall,

both proposed methods, with very low reduction orders (3–6), achieve significant speedup over the FDM solver with negligible accuracy loss, making them highly suitable for stochastic EM analysis and EM-aware optimization.

Furthermore, we demonstrate that the speedups of both *ExtRaKrylovEM* and *EiRaKrylovEM* over FDM scale *linearly* with the number of analysis time steps, highlighting the superior scalability of our proposed methods. Fig. 4 shows the runtime comparison of the proposed *ExtRaKrylovEM* and *EiRaKrylovEM* against the FDM solver [18] on the 500-segment interconnect under varying numbers of analysis time steps. The optimal configuration for *ExtRaKrylovEM* is $\{q^*, \eta_{\text{nuc}}^*, \eta_{\text{post}}^*\} = \{6, 0.5, 1.0\}$, and for *EiRaKrylovEM* is $\{q^*, \eta_{\text{nuc}}^*, \eta_{\text{post}}^*\} = \{6, 0.4, 7.0\}$.

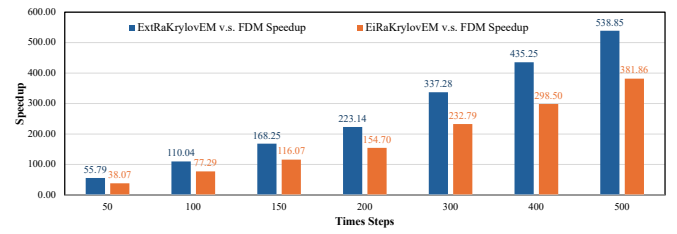


Fig. 4: Comparison between our proposed *ExtRaKrylovEM* and *EiRaKrylovEM* with Back Euler based FDM under different analysis time steps for 500 segment wire.

As shown in the figure, the speedup over FDM increases linearly with the number of time steps for both methods, reaching up to 300–500 \times with 500 time steps. This **exceptional scalability** arises because the FDM solver must perform time stepping at each time point, whereas both Krylov-based methods only need to construct the reduced-order model once and can subsequently evaluate at any time point with negligible additional cost due to the small model order. This characteristic makes them particularly advantageous for applications requiring fine temporal resolution or extended aging analysis. We also observe that *ExtRaKrylovEM* is faster than *EiRaKrylovEM* for the same number of time steps, while both methods maintain near-zero error in nucleation time and resistance change, demonstrating that scalability does not come at the cost of accuracy. Note that we did not compare with FastEM here because it does not achieve comparable accuracy under any order setting in this case.

Fig. 5 illustrates representative stress maps generated by *ExtRaKrylovEM* and *EiRaKrylovEM* under the baseline configuration $\{\eta_{\text{nuc}}, \eta_{\text{post}}, q\} = \{1, 1, 6\}$ with $\sigma_{\text{crit}} = 10^8$ Pa on a synthesized 10 segment wire. The corresponding results obtained from the FDM-based solver [18] are shown at the top for reference. Stress distributions at three representative time points are presented: around the nucleation instant (left), the mid post-void stage (center), and the end of the post-void phase (right). As can be seen from the figure, the stress maps produced by the three methods are visually indistinguishable across all stages. Quantitatively, *ExtRaKrylovEM* yields a nucleation-time error of only 0.4% and a resistance-change error of 0.00%, as shown in the bottom panel. Similar accuracy is achieved by *EiRaKrylovEM*.

TABLE II: Performance Comparison among the proposed *ExtRaKrylovEM* and existing FDM [18] and FastEM [30] methods with 100 simulation time steps.

Design	# of Segments	Methods										
		FDM [18]		Krylov-based FastEM [30]			Proposed <i>ExtRaKrylovEM</i>					
		Runtime (s)	Model Order	ϵ_{nuc}	ϵ_{post}	Runtime (s)	Config*	ϵ_{nuc}	ϵ_{post}	Total Error	Runtime (s)	Speedup to FDM
Synthesized Power Grids	100	2.01	50	64.75%	0.00%	0.15	{4, 1.0, 1.0}	0.01%	0.00%	0.01%	0.035	57.22 \times 4.29 \times
	200	13.92	50	3.86%	0.00%	0.42	{4, 1.1, 1.0}	0.06%	0.00%	0.06%	0.171	81.30 \times 2.43 \times
	500	132.31	50	0.25%	0.00%	2.23	{6, 0.5, 1.0}	0.02%	0.00%	0.02%	1.172	112.94 \times 1.90 \times
	1000	914.39	50	12.65%	0.00%	10.04	{6, 0.5, 1.0}	0.00%	0.00%	0.00%	7.131	128.22 \times 1.41 \times
	2000	2124.84	50	12.36%	0.01%	83.62	{4, 1.0, 1.0}	0.13%	0.00%	0.13%	60.223	35.28 \times 1.39 \times
ARM Cortex [40]	33	0.06	50	0.00%	0.00%	0.01	{6, 2.9, 1.0}	0.00%	0.00%	0.00%	0.003	18.74 \times 3.71 \times
IBM Power Grid Benchmarks [41]	236	21.07	50	1.29%	0.00%	0.52	{6, 9.0, 1.0}	0.00%	0.00%	0.00%	0.213	98.85 \times 2.43 \times
	572	286.24	50	0.97%	0.00%	3.64	{6, 0.3, 1.0}	0.02%	0.00%	0.02%	1.514	189.11 \times 2.40 \times
	1275	489.78	50	4.64%	0.00%	21.07	{4, 3.0, 1.0}	0.00%	0.00%	0.00%	13.468	36.37 \times 1.56 \times
	2403	3193.55	50	4.93%	0.00%	112.08	{5, 0.2, 1.0}	0.00%	0.00%	0.00%	92.268	34.61 \times 1.22 \times
Average	832	717.82	50	5.94%	0.00%	23.38	-	0.02%	0.00%	0.02%	17.620	79.26\times 2.27\times

*Config = {Krylov order, nucleation shift factor, post-void shift factor}.

TABLE III: Performance comparison between FDM [18] and the proposed *EiRaKrylovEM* using 100 simulation time steps.

Design	# of Segments	FDM Runtime (s)	Config*	ϵ_{nuc}	ϵ_{post}	Total Error	EiRaKrylovEM Runtime (s)	Speedup to FDM
Synthesized Power Grids	100	2.01	{6, 3.4, 11.0}	0.02%	0.00%	0.02%	0.040	45.75 \times
	200	13.92	{4, 0.2, 4.2}	0.03%	0.00%	0.03%	0.270	51.19 \times
	500	132.31	{6, 0.4, 7.0}	0.01%	0.00%	0.01%	1.720	77.11 \times
	1000	914.39	{5, 3.0, 2.0}	0.01%	0.00%	0.01%	11.175	81.82 \times
	2000	2124.84	{6, 0.6, 0.5}	0.08%	0.00%	0.08%	113.526	18.72 \times
ARM Cortex-M0 [40]	33	0.06	{5, 1.2, 2.5}	0.01%	0.00%	0.01%	0.019	3.41 \times
IBM Power Grid Benchmarks [41]	236	21.07	{6, 0.5, 3.5}	0.12%	0.00%	0.12%	0.367	57.42 \times
	572	286.24	{6, 0.8, 1.0}	0.04%	0.00%	0.04%	2.338	122.43 \times
	1275	489.78	{5, 3.0, 1.0}	0.01%	0.00%	0.01%	23.234	21.08 \times
	2403	3193.55	{4, 1.2, 5.0}	0.06%	0.00%	0.06%	164.238	19.44 \times
Average	832	717.82	-	0.04%	0.00%	0.04%	31.69	49.84\times

*Config = {Krylov order, nucleation shift factor, post-void shift factor}.

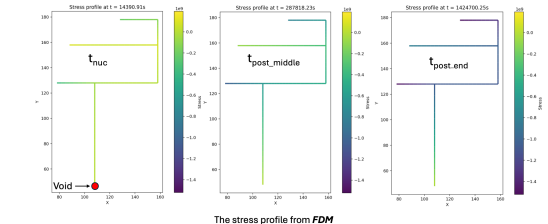
VII. CONCLUSION

In this paper, we presented two fast EM stress analysis techniques based on *rational Krylov* subspace reduction for electromigration (EM) reliability analysis of VLSI interconnects. Unlike traditional Krylov subspace methods, which can be viewed as expansion at infinite time (frequency of 0), the rational Krylov subspace allows expansion at specific time constants aligned with application metrics such as nucleation time. We explored two simulation frameworks: *ExtRaKrylovEM* based on the extended rational Krylov subspace method in the frequency domain, and *EiRaKrylovEM* based on rational Krylov exponential integration in the time domain. We demonstrated that the accuracy of both methods is sensitive to the selection of expansion point or shift time, and showed that good shift times are typically close to times of interest such as nucleation time or steady-state time. To further improve fidelity, we developed a coordinate descent optimization method to identify optimal reduction orders and shift times for both nucleation and post-void phases. Experimental results on synthesized structures and industry designs demonstrate that *ExtRaKrylovEM* and *EiRaKrylovEM* achieve orders-of-magnitude improvements in both efficiency and accuracy. Specifically, using only 4–6 reduction orders, our methods deliver sub-0.1% error in nucleation time and resistance change predictions while providing 20–500 \times speedup over finite-difference solutions depending on the number of simulation steps. In stark contrast, standard extended Krylov methods

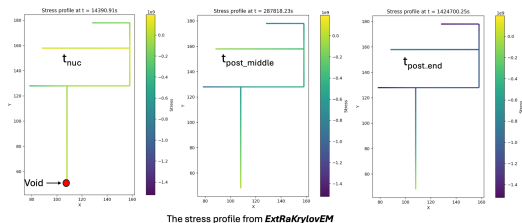
require 50+ orders yet still exhibit 10–20% nucleation time errors, rendering them impractical for EM-aware optimization and stochastic EM analysis.

REFERENCES

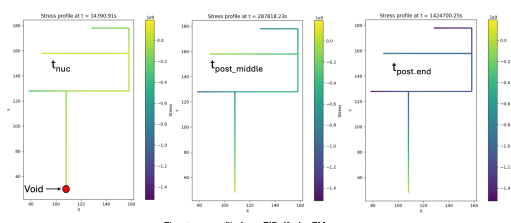
- [1] J. R. Black. Electromigration-A Brief Survey and Some Recent Results. *IEEE Trans. on Electron Devices*, 16(4):338–347, Apr. 1969.
- [2] I. A. Blech. Electromigration in thin aluminum films on titanium nitride. *Journal of Applied Physics*, 47(4):1203–1208, 1976.
- [3] M. Hauschildt, C. Hennesthal, G. Talut, O. Aubel, M. Gall, K.B. Yeap, and E. Zschech. Electromigration early failure void nucleation and growth phenomena in cu and cu(mn) interconnects. pages 2C.1.1–2C.1.6, 2013.
- [4] Valeriy Sukharev. Beyond black’s equation: Full-chip em/sm assessment in 3d ic stack. *Microelectronic Engineering*, 120:99–105, 2014.
- [5] M. A. Korhonen, P. Boergesen, K. N. Tu, and C.-Y. Li. Stress evolution due to electromigration in confined metal lines. *Journal of Applied Physics*, 73(8):3790–3799, 1993.
- [6] RL De Orio, Hajdin Ceric, and Siegfried Selberherr. Physically based models of electromigration: From black’s equation to modern tcad models. *Microelectronics Reliability*, 50(6):775–789, 2010.
- [7] Xin Huang, Armen Kteyan, Sheldon X.-D. Tan, and Valeriy Sukharev. Physics-based electromigration models and full-chip assessment for power grid networks. *IEEE Trans. on Computer-Aided Design of Integrated Circuits and Systems*, 35(11):1848–1861, 2016.
- [8] Valeriy Sukharev, Armen Kteyan, and Xin Huang. Postvoiding stress evolution in confined metal lines. *IEEE Trans. on Device and Materials Reliability*, 16(1):50–60, 2016.
- [9] H. Chen, S. X.-D. Tan, X. Huang, T. Kim, and V. Sukharev. Analytical modeling and characterization of electromigration effects for multibranch interconnect trees. *IEEE Trans. on Computer-Aided Design of Integrated Circuits and Systems*, 35(11):1811–1824, 2016.
- [10] Vivek Mishra and Sachin S. Sapatnekar. Predicting electromigration mortality under temperature and product lifetime specifications. In *Proc. Design Automation Conf. (DAC)*, pages 1–6, 2016.



(a) Post void stress distribution obtained from FDM [18] under different time points.



(b) Post void stress distribution obtained from the proposed *ExtRaKrylovEM* under different time points.



(c) Post void stress distribution obtained from the proposed *EiRaKrylovEM* under different time points.

Fig. 5: Accuracy comparison with the finite difference method [18] at different times. Red dot indicates the nucleated cathode node

- [11] H.-B. Chen, S. X.-D. Tan, J. Peng, T. Kim, and J. Chen. Analytical modeling of electromigration failure for vlsi interconnect tree considering temperature and segment length effects. *IEEE Transaction on Device and Materials Reliability (T-DMR)*, 17(4):653–666, 2017.
- [12] Sandeep Chatterjee, Valeriy Sukharev, and Farid N. Najm. Power grid electromigration checking using physics-based models. *IEEE Trans. on Computer-Aided Design of Integrated Circuits and Systems*, 37(7):1317–1330, 2018.
- [13] C. Cook, Z. Sun, E. Demircan, M. D. Shroff, and S. X.-D. Tan. Fast electromigration stress evolution analysis for interconnect trees using krylov subspace method. *IEEE Trans. on Very Large Scale Integration (VLSI) Systems*, 26(5):969–980, May 2018.
- [14] S. Wang, Z. Sun, Y. Cheng, S. X.-D. Tan, and M. Tahoori. Leveraging recovery effect to reduce electromigration degradation in power/ground TSV. In *Proc. Int. Conf. on Computer Aided Design (ICCAD)*, pages 811–818. IEEE, Nov. 2017.
- [15] H. Zhao and S. X.-D. Tan. Postvoiding fem analysis for electromigration failure characterization. *IEEE Trans. on Very Large Scale Integration (VLSI) Systems*, 26(11):2483–2493, Nov. 2018.
- [16] Ali Abbasinasab and Małgorzata Marek-Sadowska. RAIN: A tool for reliability assessment of interconnect networks—physics to software. In *Proc. Design Automation Conf. (DAC)*, pages 133:1–133:6, New York, NY, USA, 2018. ACM.
- [17] L. Chen, S. X.-D. Tan, Z. Sun, S. Peng, M. Tang, and J. Mao. Fast analytic electromigration analysis for general multisegment interconnect wires. *IEEE Transactions on Very Large Scale Integration (VLSI) Systems*, pages 1–12, 2019.

- [18] Z. Sun, S. Yu, H. Zhou, Y. Liu, and S. X.-D. Tan. EMSpice: Physics-Based Electromigration Check Using Coupled Electronic and Stress Simulation. *IEEE Transactions on Device and Materials Reliability*, 20(2):376–389, June 2020.
- [19] Mohammad Abdullah Al Shohel, Vidya A. Chhabria, Nestor Evmoropoulos, and Sachin S. Sapatnekar. Analytical modeling of transient electromigration stress based on boundary reflections. In *Proc. Int. Conf. on Computer Aided Design (ICCAD)*, pages 1–8, 2021.
- [20] Sheldon X.-D. Tan, Mehdi Tahoori, Taeyoung Kim, Shengcheng Wang, Zeyu Sun, and Saman Kiamehr. *VLSI Systems Long-Term Reliability – Modeling, Simulation and Optimization*. Springer Publishing, 2019.
- [21] Pavlos Stoikos, George Floros, Dimitrios Garyfallou, Nestor Evmoropoulos, and George Stamoulis. Electromigration stress analysis with rational krylov-based approximation of matrix exponential. In *2023 19th International Conference on Synthesis, Modeling, Analysis and Simulation Methods and Applications to Circuit Design (SMACD)*, pages 1–4, 2023.
- [22] S. P. Hau-Riege and C. V. Thompson. Experimental characterization and modeling of the reliability of interconnect trees. *Journal of Applied Physics*, 89(1):601–609, 2001.
- [23] Xiaoyi Wang, Shaobin Ma, Sheldon X.-D. Tan, Chase Cook, Liang Chen, Jianlei Yang, and Wenjian Yu. Fast physics-based electromigration analysis for full-chip networks by efficient eigenfunction-based solution. *IEEE Transactions on Computer-Aided Design of Integrated Circuits and Systems*, 40(3):507–520, 2021.
- [24] Sandeep Chatterjee, Valeriy Sukharev, and Farid N. Najm. Fast physics-based electromigration checking for on-die power grids. In *Proc. Int. Conf. on Computer Aided Design (ICCAD)*, pages 1–8, 2016.
- [25] Farid N. Najm and Valeriy Sukharev. Efficient simulation of electromigration damage in large chip power grids using accurate physical models (invited paper). In *2019 IEEE International Reliability Physics Symposium (IRPS)*, pages 1–10, 2019.
- [26] A. C. Antoulas. *Approximation of Large-Scale Dynamical Systems*. The Society for Industrial and Applied Mathematics (SIAM), 2005.
- [27] Sheldon X.-D. Tan and L. He. *Advanced Model Order Reduction Techniques in VLSI Design*. Cambridge University Press, 2007.
- [28] J. M. Wang and T. V. Nguyen. Extended Krylov subspace method for reduced order analysis of linear circuit with multiple sources. In *Proc. Design Automation Conf. (DAC)*, pages 247–252, 2000.
- [29] {Mikhail A.} Bochev. *A short guide to exponential Krylov subspace time integration for Maxwell's equations*. Number 1992 in Memorandum. University of Twente, Netherlands, September 2012.
- [30] Chase Cook, Zeyu Sun, Ertugrul Demircan, Mehul D. Shroff, and Sheldon X.-D. Tan. Fast Electromigration Stress Evolution Analysis for Interconnect Trees Using Krylov Subspace Method. *IEEE Trans. on Very Large Scale Integration (VLSI) Systems*, 26(5):969–980, May 2018.
- [31] Mikhail A. Botchev. Krylov subspace exponential time domain solution of maxwell's equations in photonic crystal modeling. *Journal of Computational and Applied Mathematics*, 293:20–34, 2016. Efficient Numerical Methods for Large-scale Scientific Computations.
- [32] Hao Zhuang, Wenjian Yu, Shih-Hung Weng, Ilgweon Kang, Jeng-Hau Lin, Xiang Zhang, Ryan Coutts, and Chung-Kuan Cheng. Simulation algorithms with exponential integration for time-domain analysis of large-scale power delivery networks. *IEEE Transactions on Computer-Aided Design of Integrated Circuits and Systems*, 35(10):1681–1694, 2016.
- [33] Pavlos Stoikos, George Floros, Dimitrios Garyfallou, Nestor Evmoropoulos, and George Stamoulis. Electromigration stress analysis with rational krylov-based approximation of matrix exponential. In *Synthesis, Modeling, Analysis and Simulation Methods and Applications to Circuit Design (SMACD)*, pages 1–4, 2023.
- [34] M A Korhonen, P Borgesen, K N Tu, and C Y Li. Stress evolution due to electromigration in confined metal lines. *Journal of Applied Physics*, 73(8):3790–3799, 1993.
- [35] Valeriy Sukharev, Armen Kteyan, and Xin Huang. Postvoiding stress evolution in confined metal lines. *IEEE Trans. on Device and Materials Reliability*, 16(1):50–60, 2016.
- [36] Sandeep Chatterjee, Valeriy Sukharev, and Farid N. Najm. Fast Physics-Based Electromigration Checking for On-Die Power Grids. In *Proceedings of the 35th International Conference on Computer-Aided Design, ICCAD '16*, pages 1–8, New York, NY, Nov. 2016. ACM Press.
- [37] X. Huang, A. Kteyan, S. X.-D. Tan, and V. Sukharev. Physics-Based Electromigration Models and Full-Chip Assessment for Power Grid Networks. *IEEE Trans. on Computer-Aided Design of Integrated Circuits and Systems*, 35(11):1848–1861, 2016.

- [38] V. Sukharev, X. Huang, and S. X.-D. Tan. Electromigration induced stress evolution under alternate current and pulse current loads. *Journal of Applied Physics*, 118(3):034504, 07 2015.
- [39] Wentian Jin, Liang Chen, Sheriff Sadiqbatcha, Shaoyi Peng, and Sheldon X.-D. Tan. Emgraph: Fast learning-based electromigration analysis for multi-segment interconnect using graph convolution networks. In *2021 58th ACM/IEEE Design Automation Conference (DAC)*, pages 919–924, 2021.
- [40] AMD Limited. Cortex-m0 technical reference manual. Online, 2009. Accessed: Feb. 2019.
- [41] Sani R. Nassif. Power grid analysis benchmarks. In *Proc. Asia South Pacific Design Automation Conf. (ASPDAC)*, page 376–381, 2008.